Paper

Induced Surge Characteristics from a Counterpoise to an Overhead Loop Circuit

Toshio Sonoda* Member
Yasuo Takeuchi* Member
Shozo Sekioka** Member
Naoto Nagaoka*** Member
Akihiro Ametani*** Member

This paper surveys disturbances experienced in the low-voltage control circuits of the power stations and the substations of Kansai Electric Power. Induced voltages to an overhead control cable from a grounding mesh were measured when an impulse current was applied to the grounding mesh. A non-metallic sheath cable (CVV cable) and a cable with a metallic sheath (CVV-S cable) were tested to investigate the effect of the metallic sheath on the induced voltage to the cable. Then, a simulation model of the transient induced voltage to the overhead conductor from a counterpoise was proposed. Finally, the simulation results were compared with the measured results to confirm the accuracy of the proposed method.

Keywords: counterpoise, inducing characteristic, distributed-parameter circuit, low-voltage control circuit, grounding mesh

1. Introduction

Disturbances and malfunctions in the low-voltage control circuits are on the increase compared to those in the main circuits in power systems. This corresponds to an increase in the low-voltage digital circuits and a demand for power-saving. Furthermore, the development of telecommunication tools and their wide usage results in problems in telecommunication equipment in factories, buildings, and homes. The disturbances are caused by lightning surges, coming both directly from the power and telecommunication circuits, and indirectly from a grounding circuit. The surge incoming route has not been made clear. This is because the power, telecommunication and grounding circuits are very complicated, and the configuration of the equipment is different in each case. Thus, guessing is the only way to estimate the cause of the problems and the incoming route.

Several case studies on a grounding resistance and an induced surge from a main circuit to a low-voltage control circuit are available [1]~[8]. However, the incoming route to the low-voltage circuit has yet to be made clear. In-depth investigation is needed. It is known that there are two routes from the main power circuit to the low-voltage control circuit - one, from a counterpoise and a grounding mesh, and the other, from a potential divider (PD) and a current transformer (CT). The number of surges coming in through the counterpoise has been estimated as roughly half the total number of lightning surges.

The authors studied the grounding resistance characteristics of a counterpoise in a substation [9]~[13], and proposed a circuit model for a lighting surge analysis [12][13]. This paper surveys disturbances experienced in the low-voltage control circuits of the power stations and the substations of Kansai Electric Power. Induced voltages to an overhead control cable from a grounding mesh were measured when an impulse current was applied to the grounding mesh. A non-metallic sheath cable (CVV cable-multicore) and a cable with a metallic sheath (CVV-S cable-multicore) were tested to investigate the effect of the metallic sheath on the induced voltage to the cable core, and also the effect of the core of the CVV cable grounded to the counterpoise. Next, a simulation model of the transient induced voltage to the overhead conductor from a couterpoise was proposed. This was based on the distributed-parameter circuit theory [14]. And finally, the simulation results were compared with the measured results to confirm the accuracy of the proposed method.

2. Investigated Results of Disturbances

The rate of disturbances in the low-voltage control circuits and in the telecommunication circuits caused by a lightning surge amounts to approximately 75% of the total output of Kansai Electric Power between 1982 and 1986. The circuits on which the disturbances have been estimated to occur are shown in Fig. 1. The circuit

* General R&D Center, The Kansai Electric Power Co., Inc.
3-11-20, Nakoji, Amagasaki 661-0974
** R&D Group, Kansai Tech Corp.
3-1-176 Fukusaki, Minato-ku, Osaka 552-0013
*** Department Electrical Engineering , Doshisha University
1-3, Tatara, Kyotanabe 610-0321

classification is, according to JEC-210, "Dielectric test voltages for low-voltage control circuits in power stations and substations" [15]. A number of disturbances were observed in "Circuit category 8" and "Others" (more than 56%). "Category 8" was the circuit in which the voltage was less than DC/AC 60 V. It involved electronics, telecommunication equipment, and signal circuits. "Others were those that were not classified in the standard with JEC-210. It included auxiliary circuits, water level meters in a hydro power station, invader detecting circuits, and ITV circuits in a substation.

Investigations done on the incoming route of a lightning surge in the disturbances revealed two routes - one, from a main power circuit via the PD, and the other, from a grounding mesh due to a discharge of a lightning arrestor, and from a ground wire. The number of disturbances from the routes (Fig. 2) via the PD and from the grounding system were nearly the same; about 20% each.

The cause of overvoltage in the low-voltage control circuits, due to a lightning surge from transmission lines to substations and power stations, could be described as follows:

(a) Transfer voltage of the PD (include CT) (V_{sec}).

(b) Induced voltage from the grounding mesh to the control cable, due to a discharge of a lighting arrestor and from a ground wire (V_{ind}).

(c) The electrical potential oscillation of the PD due to a surge current to the grounding mesh (V_{gPD}).

(d) The electrical potential oscillation of the control panel due to a surge current to the grounding mesh (V_{gCN}).

The equation for overvoltage V_{cc} in the low-voltage control circuits is as follows:

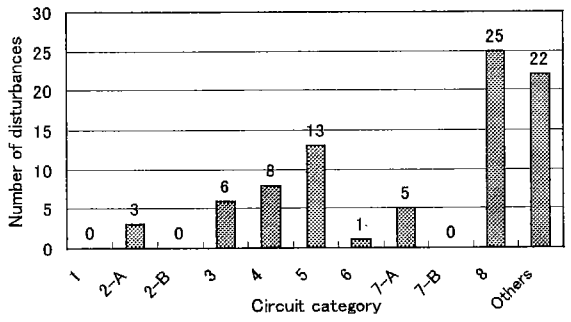

Fig. 1. Disturbances that took place

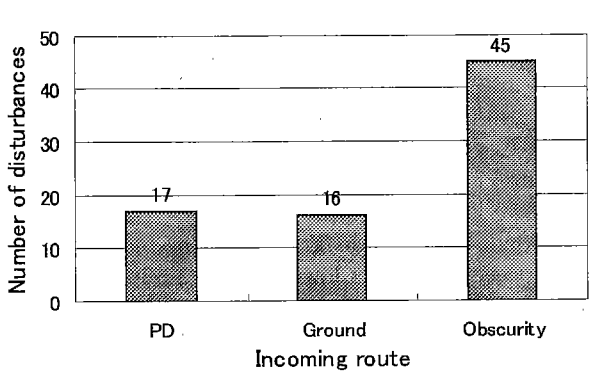

Fig. 2. Disturbances by incoming route

$$V_{cc} = V_{sec} + V_{ind} + V_{gPD} + V_{gCN} \quad \cdots\cdots\cdots\cdots \quad (1)$$

Of these, the magnitude of V_{sec} and V_{ind} were large. The transfer voltage V_{sec} mainly occurred in the circuit of the PD and the CT. The induced voltage V_{ind} from the grounding mesh is discussed as majority and common induced voltage that occurs in a low-voltage control circuit.

3. Inducing Characteristics from a Counterpoise to a Low-voltage Contorol Cable

Investigation revealed that in a low-voltage control circuit the disturbance occurred in the PD secondary circuit or from the grounding mesh, in the form of overvoltage. The usage of CVV-S cables was effective in reducing overvoltage to be the countermeasure. They were mainly used in the extra-high-voltage substations grounding at both ends, CVV cables were used in the distribution substation. The sheaths of the CVV-S cables were grounded at one side in a hydro power station. Since potential differences would occur between the equipment side (outdoors) and the control panel side (indoors) due to the grounding mesh, the two of grounding mesh were separated in a hydro power station. Thus, two types of cables, both of different grounding ways, were used in the substations and the power stations.

Next, the measurement of the induced voltage from a counterpoise to a low-voltage control cable was carried out for the purpose of investigating the inducing characteristic and ensuring the grounding effect of CVV-S cables (Fig. 3). The configuration of the counterpoise was 24.8 m × 34.1 m. It composed of HDCC 60 mm^2, buried 1 m in depth. Two types of counterpoise were used for the test - one was the grounding mesh, and the other, a 34.1 m straight conductor (counterpoise) separated from the grounding mesh. The voltage between the cable core and the grounding mesh was divided by a voltage divider, converted to an optical signal and restored by an E/O and O/E converter. The voltage waveforms were measured using a digital oscilloscope. The specifications of the measuring instruments used are shown in Table 1.

The grounding resistance of the grounding mesh was found to be 4.2 Ω and that of the straight conductor, 29 Ω. The resistivity (at site 1) calculated from the grounding resistance was 250 ∼ 300 Ωm. 2-cores where the control cables CVV-S and CVV were laid on the ground at the point $X = 0$. The sheath of the CVV-S

Table 1. Specifications of measuring instruments

Measuring Instrument	Maker	Type	Specification
Pulse Generator	COSMOTEC	———	5kV, 3A
Digital Oscilloscope	Sony Tektronix	TDS-540	500MHz
E/O, O/E Convetor	Sony Tektronix	P6904A	100MHz
Current Transformer	PEARSON	MODEL-2877	Rising Time: 2ns
Passive Probe	Sony Tektronix	P6139A	500MHz
Attenuator	Sony Tektronix	———	DC∼2GHz
Impulse Generator	Nichicon	IG-3000	3MV, 450kJ
Voltage Divider	Tama Electric	Electrohm PWP	800kV, Rising Time: 80ns
High Voltage Probe	Sony Tektronix	P6009	120MHz
Current Transformer	PEARSON	MODEL-1330	Rising Time: 0.25 μs
High Voltage Attenuator	Otowa Electronics	OAT-50	1.5kV, Response: 0.1 μs

Table 2. Test cases

Power Source	Injected Current	Counter-poise	Control Cable	Switch Condition (S-R)
PG	1[A] 0.05/13 μs	Straight (29 Ω)	CVV-S	OFF-OFF
			CVV	OFF-ON
		Mesh (4.2 Ω)	CVV-S	ON -OFF
			CVV	ON -ON
IG	6.3[kA] 2.8/8 μs	Straight (29 Ω)	CVV-S	OFF-OFF
			CVV	OFF-ON
		Mesh (4.2 Ω)	CVV-S	ON -OFF
			CVV	ON -ON

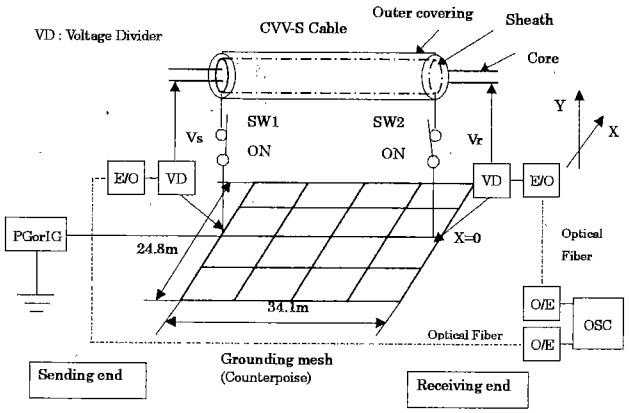

(a) CVV-S cable

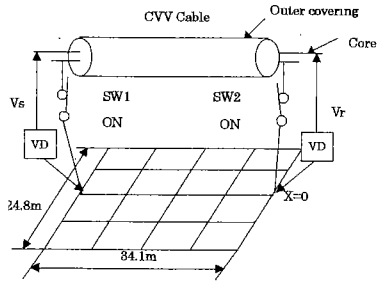

(b) CVV cable

Fig. 3. Measurement circuit for induced voltage to a control cable

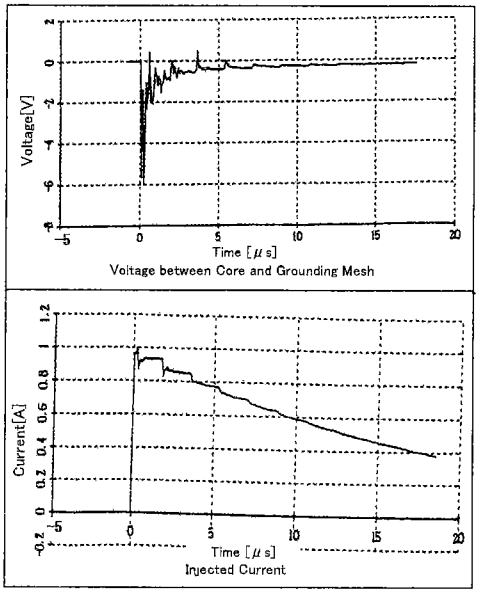

(a) PG

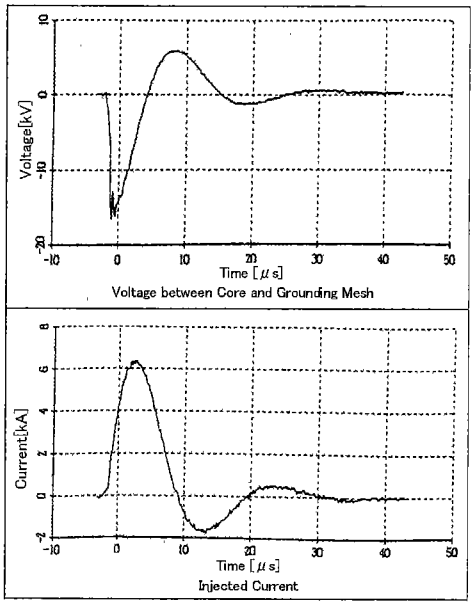

(b) IG

Fig. 4. Measured voltage and current waveforms

cable was connected to the grounding mesh by switches at the sending and the receiving ends. The voltage between the core and the counterpoise were measured on switch conditions at both ends. The spare core of the CVV cable was connected to the switches instead of the sheath of the CVV-S cable. The test cases are shown in Table 2.

Two power sources were used in this test - the pulse generator (PG), to inject steep-front current of 1 A (0.05/13 μs), and the 3MV impulse generator (IG), to inject high impulse current of 6.3 kA (2.8/8 μs). The measured voltage and current waveforms, in case of the switches at both ends being opened, are shown in Fig. 4. Note that the current waveform injected by the PG is steep upfront. The voltage waveform has a high peak value and suddenly decreases like a spike. On the other hand, the current waveform injected by the IG is slacker. The voltage waveform is steep-front compared with current one.

The measured results of an induced voltage injected by the PG and the IG are shown in Fig. 5. The ones of the CVV-S cable compared with that of the CVV cable in the case of the grounding mesh are shown in Fig. 6. These graphs indicate the peak value of the induced voltage.

From Fig. 5(a), note that the induced voltage between the core and the straight conductor was higher than that of the grounding mesh. This is because the grounding resistance of the straight conductor was high. This trend was also evident in the case of the CVV cable and the CVV-S cable (Figs. 5(a) and (b)). From Fig. 5(b), it is also evident that the peak value of the induced voltage injected by the IG was lower than that injected by the PG. This was because the wavefront of the injected current by IG (2.8 μs) was slacker than that injected by the PG (0.05 μs).

From Fig. 6, it is evident that the CVV-S cable had

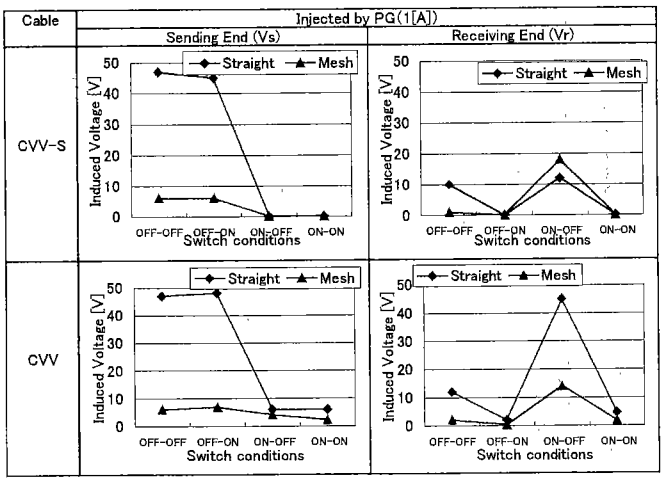

(a) Injected by PG (1 [A])

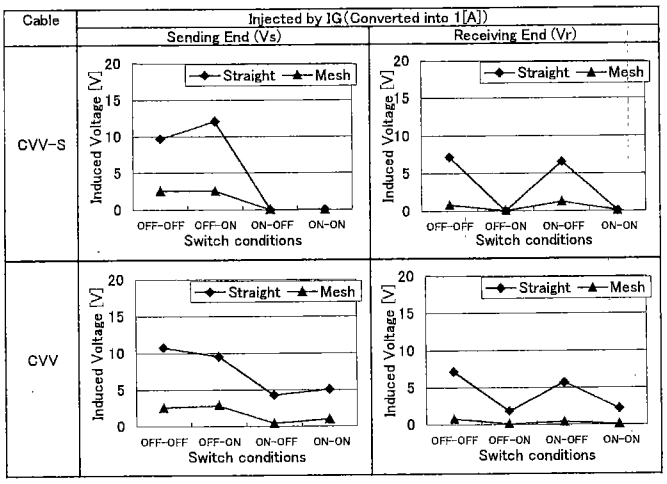

(b) Injected by IG (converted into 1 [A])

Fig. 5. Measurement results of induced voltage to a control cable (1)

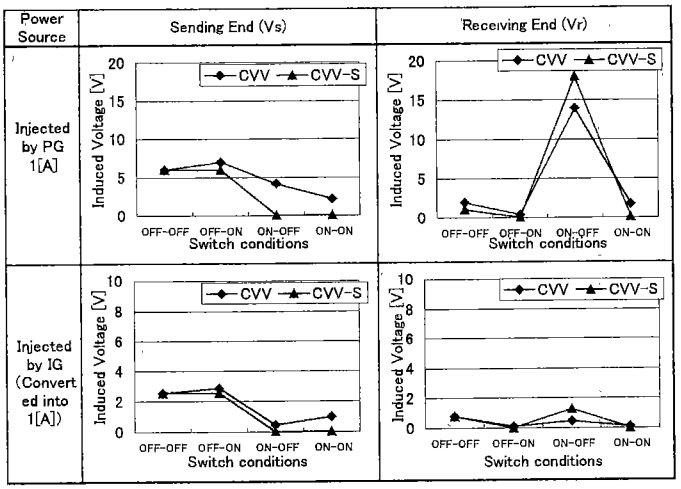

Fig. 6. Measurement results of induced voltage to a control cable (2)

the ability to reduce the voltage difference between cable core and grounding mesh in the case of both ends being grounded. Further, the CVV-S cable had a more severe effect than the CVV cable when the SW1 was closed and SW2 was opened. The CVV cable had the effect to reduce the voltage difference between cable core and grounding mesh when the spare core was grounded at both ends.

Table 3. Comparison with reference [16]

		This Paper		Reference [16]	
Grounding Mesh		24.8×34.1m(HDCC60sq)		28×200m(HDCC55sq)	
Depth		1m		0.7m	
Resistivity		250～300[Ωm]		400～600[Ωm]	
Grounding Resistance		4.2[Ω]		2.4～3.6[Ω]	
Control Cable		CVV-S 2C×3.5sq×30m		CVV-S 4C×8sq×130m	
		CVV 2C×3.5sq×30m		CVV 4C×8sq×130m	
IG	Injected Current	6300[A](2.8×8μS)		1237[A](0.5×60μS)	
	Voltage [V]	SE [V]	RE [V]	SE [V]	RE [V]
	CVV-S	210	180	(*1)264	(*1)290
	CVV-S(1[A])	0.033	0.029	0.042	0.046
	CVV	16000	5000	(*1)17640	(*1)8064
	CVV(1[A])	2.54	0.79	2.80	1.28
PG	Injected Current	1[A](0.05×13μS)			
	Voltage [V]	SE [V]	RE [V]		
	CVV-S	0.07	0.10		
	CVV	7.00	0.38		

SE : Sending End
RE : Receiving End
*1: Converted into 6.3[kA]

Some measured results of induced voltage in a low-voltage control circuit at a substation and power station were reported [16]. But these were dependent on the measurement conditions, the waveform of the injected current, the injected point, the configuration of the grounding mesh, the ground resistivity, and so on. A similar measured result obtained at the Akagi testing center of CRIEPI was compared with this result and is shown in Table 3. It could be understood that the induced voltages in the control cable were of almost the same value.

The grounding condition of the cable sheath affected the voltage difference between the core and the counterpoise. The voltage at the sending end V_s depended on SW1, and at the receiving end V_r depended on SW2 (Figs. 5 and 6). In the case when SW1 was open, V_s had a high value, due to the coupling between core, sheath, and counterpoise was a small. On the contrary, in the case when SW1 was closed, V_s had a low value, as there was a large coupling between the sheath and the counterpoise.

It is considered that the voltage potential of the cable sheath and cable core could be used to explain the propagation phenomenon of induced voltage in a low-voltage control circuit. The induced voltage and voltage difference between the cable core and grounding mesh were caused by an increase in the ground potential, which in turn was due to the current that flowed through the grounding mesh and cable sheath, and static and magnetic coupling between the cable sheath and core. The voltage difference between the cable core and grounding mesh was explained using the voltage traveling through the cable sheath and the induced voltage traveling through the cable core, as shown in Fig. 7(a) ～ (d).

In the case when both ends of the cable sheath were grounded as shown in Fig. 7(a), ① the surge current injected into the grounding mesh and the ground potential

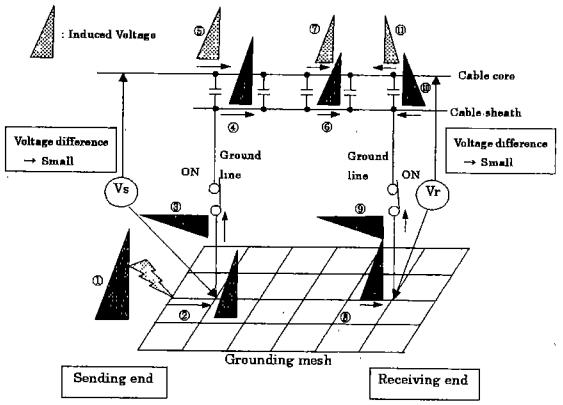

(a) Propagation of voltage and current (both ends grounded)

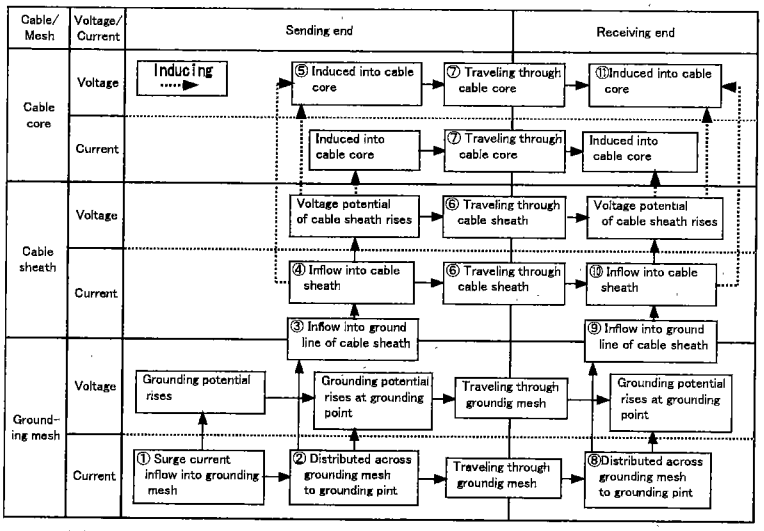

(b) Process of induced voltage into cable core (both ends grounded)

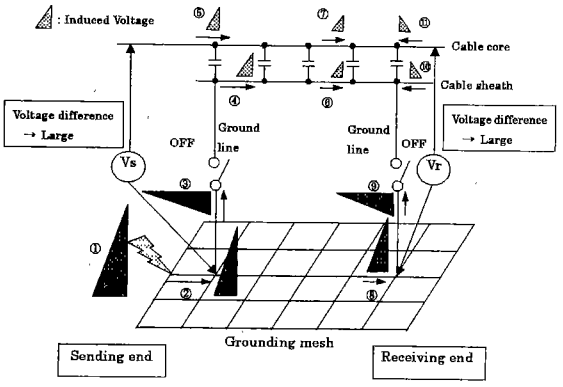

(c) Propagation of voltage and current (both ends open)

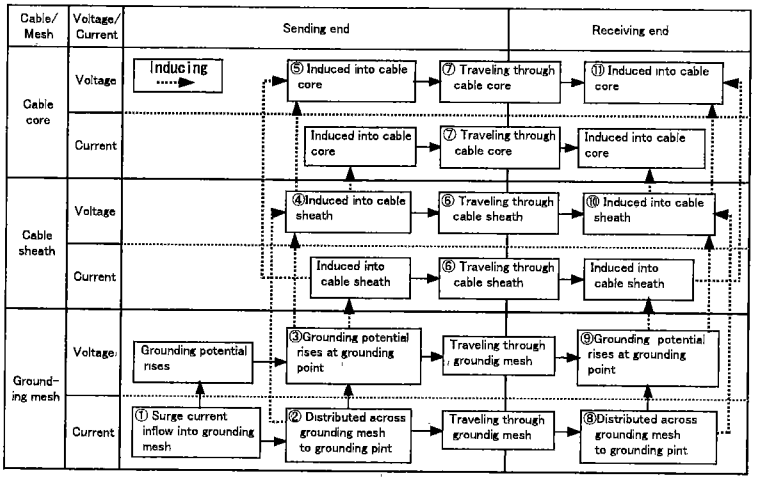

(d) Process of induced voltage into cable core (both ends open)

Fig. 7. Conception of an induced voltage into a control cable

suddenly rose at the wavefront, ② the current was distributed and it traveled through the grounding mesh; and the voltage also traveled, ③ the current reached the grounding point and flowed into the ground line of the cable sheath, ④ the current flowed into the cable sheath and the voltage potential rose, ⑤ the voltage was induced into the cable core due to static and magnetic coupling between the cable sheath and core, ⑥ the voltage in the cable sheath and ⑦ the induced voltage in the cable core traveled to the other side of the cable. It could be considered that the attenuation of the voltage that traveled through the cable sheath and core was small in case of the cable was short.

On the other hand, ⑧ the current distributed across the grounding mesh and the voltage reached another grounding point, ⑨ the current flowed into the ground line of the cable sheath, ⑩ the current flowed into the cable sheath, and the voltage potential rose, ⑪ the voltage was induced in the cable core due to static and magnetic coupling between the cable sheath and core. The wavefront value of the voltage that was measured at the receiving end of the grounding mesh was lower than that at the sending end, but the value at the wavetail was almost the same as that at the sending end.

Thus, at the receiving end, the voltage value was determined by the voltage potential of the cable sheath and the induced voltage in the cable core from the receiving end, both of which traveled from the sending end to the receiving end. The voltage between the cable core and the grounding mesh at the sending and the receiving ends could be decided by the condition of switches (coupling coefficient between the grounding mesh, the cable sheath, and the core). In the case when coupling between the core and the grounding mesh was large, there were slight differences in the voltage between the core and the grounding mesh. This is a major advantage in terms of the insulation. Because the protection relays, meters and various device are connected between the cable core and grounding mesh. It is said that the CVV-S cable has the ability to reduce the voltage difference between cable core and grounding mesh when the cable sheath is grounded at both ends. However, it is also said that when the cable sheath is grounded at the injected point, and not grounded at the other side, the CVV-S cable has no effect on the surge. Thus, overvoltage was caused at the other side due to the reflection

(Fig. 5 and 6, receiving end, SW condition ON-OFF).

The overvoltage occurred in the case when SW1 was closed and SW2 opened, especially when the steep-front current was injected by the PG (Fig. 6). When neither the CVV cable nor the CVV-S cable was grounded, the potential rise of the grounding mesh was found to affect the insulation of the cable and the various devices directly. But it was possible to reduce the voltage difference between cable core and grounding mesh by having the cable sheath of the CVV-S cables and the spare core of the CVV cables grounded at both ends. This effect reduced the voltage difference more than two times when spare core of the CVV cable was grounded compared with that was not grounded.

4. EMTP Simulation

4.1 Basic Theory—Impedance and Admittance The transient phenomenon could be calculated by using a multi-phase distributed-parameter circuit composed of insulated underground and overhead lines. This requires the condition that ① the overhead and underground lines were horizontal against the ground, ② the lines were of equal length, and ③ the effect at the ends were negligible. The ground is not a complete conductor. An assumption of complete conductor was found to be unreal and meaningless in the case of the grounding circuit. Under the conditions, the voltage and current of the overhead "n" conductors and the underground "m" conductors of the multi-phase distributed-parameter circuit are given in the following formulas [14].

$$\left.\begin{aligned} d^2(V)/dx &= [Z][Y](V) \\ d^2(I)/dx &= [Y][Z](I) \end{aligned}\right\} \quad \cdots\cdots\cdots\cdots\cdots (2)$$

where (V), (I): Vector of voltage and current of "$n+m$" conductor at location x

$[Z][Y] = ([Y][Z])^t$ is formed.

$[Z]$ and $[Y]$ are a series impedance matrix and a shunt admittance matrix of multi-phase distributed parameter lines, respectively. Each element is given in the following equation [14]:

$$\left.\begin{aligned} Z_{ij} &= Z_{cij} + Z_{eij}, Z_{cij} = 0 : i \neq j \\ [Y] &= j\omega 2\pi\varepsilon [P]^{-1} \end{aligned}\right\} \quad \cdots\cdots\cdots (3)$$

where $[P]$: Potential coefficient matrix

Z_c is the internal impedance of a conductor, which is given by Schelkunoff [17]. Z_e is earth return impedance. Overhead, underground, and mixed overhead-underground impedances are given by Pollaczek [18]. Carson's formula is only for the impedance of the overhead line [19]. However, since these equations are represented in an infinite integration or an infinite series, they could not be applied for analytic calculation. Practical approximate formulas are given in the following equation [14] and the configurations of the conductors are shown in Fig. 8:

(a) Internal impedance of conductor

$$\left.\begin{aligned} Z_{cii} &\fallingdotseq R_{dc}\sqrt{1 + j\omega\mu_c S/R_{dc}\cdot l_c^2} \\ Z_{cij} &= 0 : i \neq j \end{aligned}\right\} \quad \cdots\cdots\cdots (4)$$

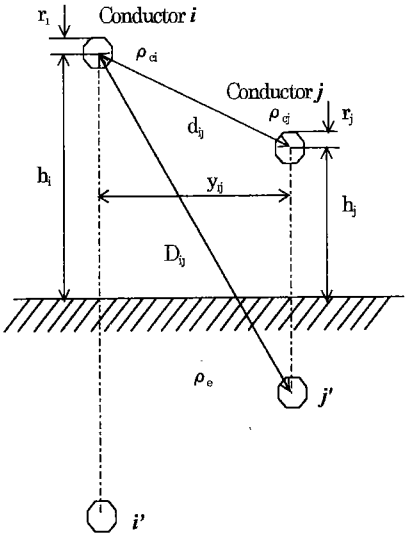

(a) Overhead line

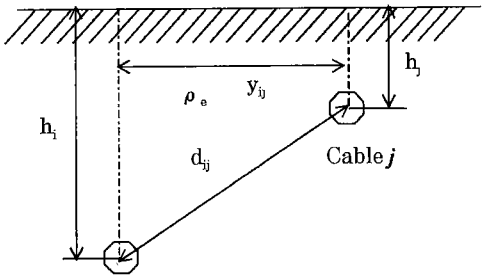

(b) Underground cable

Fig. 8. Configulation of conductors

where $R_{dc} = \rho_c/S$: DC resistance of conductor, S: Square measure, l_c: Circumference length, ρ_c: Resistivity, μ_c: Permeability

(b) Earth return impedance

(i) Overhead line [20]

$$Z_{eij} = j\omega(\mu_0/2\pi)\ln(S_{ij}/d_{ij}) \quad \cdots\cdots\cdots\cdots (5)$$

where $S_{ij} = \sqrt{(h_i + h_j + 2h_e)^2 + {y_{ij}}^2}$

$d_{ij} = \sqrt{(h_i - h_j)^2 + {y_{ij}}^2}$

$h_e = \sqrt{\rho_e/j\omega\mu_0}$

$i = j : S_{ii} \fallingdotseq 2(h_i + h_e), d_{ii} = r_i, h_i$

where h_i: Height, r_i: Radius of conductor, y_{ij}: Horizontal distance between conductors

(ii) Underground cable [14]

$$Z_{eij} = j\omega\frac{\mu_0}{2\pi}\left\{\ln\left(\frac{S_{ij}}{d_{ij}}\right) - 0.077 - \frac{2(h_i + h_j)}{3h_e}\right\} \quad \cdots\cdots\cdots\cdots (6)$$

(iii) Overhead—Underground mutual-impedance

The unit mutual-impedance of overhead conductors and a counterpoise are given in the following equation. The derivation is explained in Appendix.

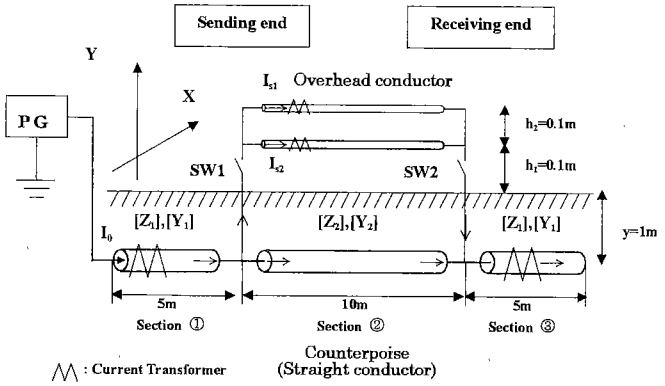

Fig. 9. Measurement circuit for induced current

$$Z_{i3} = Z_{3i} = -\frac{\rho}{\pi}\int_0^\infty \left(a - \sqrt{\alpha^2 + {m_2}^2}\right)\cos ax \times \exp\left(-\sqrt{\alpha^2 + {m_2}^2}\, y_c\right)\left(\exp\left(-ah_i\right) - 1\right) da \quad \cdots\cdots (7)$$

where ${m_2}^2 = j\omega\mu_0/\rho$, $i = 1$ and 2

It is impossible to integrate analytically the eq. (7). Therefore, the above equation is calculated numerically. The element P_{ij} of potential coefficient matrix is given in the following equations:

(c) Potential coefficient matrix

(i) Overhead line:

$$P_{ij} = \ln(D_{ij}/d_{ij}) \quad \cdots\cdots (8)$$

where $D_{ij} = \sqrt{(h_i + h_j)^2 + y_{ij}^2}$

(ii) Underground cable:

$$\left.\begin{array}{l} P_{ij} = \ln(r_{2i}/r_{1i}), \\ P_{ij} = 0 : i \neq j \end{array}\right\} \quad \cdots\cdots (9)$$

Where r_{1i}: Radius of cable core,
r_{2i}: Radius of insulation layer

Using the above impedance and admittance (a)~(c), it is possible to calculate the transient phenomenon in overhead and underground lines.

4.2 Comparison with a Measured Result

(1) Measurement Cable sheath and core voltages can be calculated by a current flowing through a counterpoise (straight conductor) and the cable sheath using the self- and mutual-impedances, and admittances. The simple measurement circuit (Fig. 9) was set up to carry out a simulation. The pulse current (2 A, 0.05/70 μs) was injected to a counterpoise from a PG (Specifications of the measuring instruments same as in Table 1). A straight conductor (HDCC 60 mm^2, length 20 m, buried 1 m depth) was used for the counterpoise. The resistivity (at site 2) calculated from the grounding resistance was about 300 Ωm. An overhead loop circuit composed of two parallel straight conductors (diameter 3 mm, length 10 m, height 0.1 and 0.2 m) was used to represent a control circuit. The both ends of the conductors were short-circuited and were then connected to the counterpoise by switches.

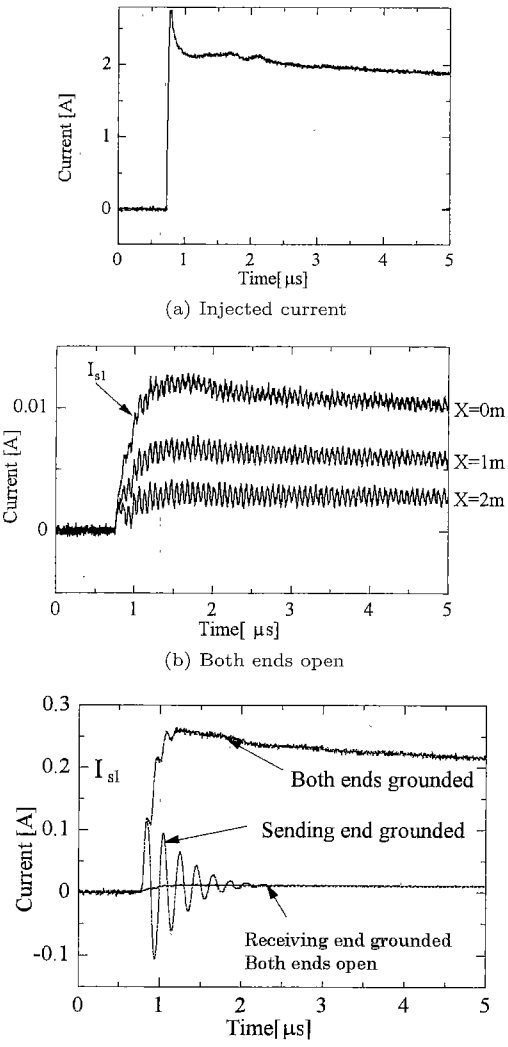

Fig. 10. Induced current in a loop circuit

The induced current to the loop circuit was measured, by changing the horizontal position of the loop circuit from the point $X = 0$ in the case of the SW1 and SW2 being opened. Measured result is shown in Fig. 10(b). The induced current is about 0.5% ($X = 0$) of the injected current and decreases as X increases. The induced current at the sending end when the switch condition is changed ($X = 0$) is shown in Fig. 10(c). When the both ends are grounded, about 12.5% of the injected current flows into the loop circuit. When SW1 is open and SW2 is closed, the induced current is the same as that in Fig. 10(b) ($X = 0$). When SW1 closed and SW2 open, the oscillated current flows in the beginning, and then convergs to the same value as that in Fig. 10(b) ($X = 0$).

(2) Simulation result For the simulation of the induced current in a loop circuit on a counterpoise (straight conductor), the distributed-parameter model is used. For a series impedance, Z_1 and shunt admittance, Y_1 of the counterpoise as shown in sections ① and ③ in Fig. 9. Figure 11 shows a π equivalent circuit in terms of unit length as shown in section ② for the

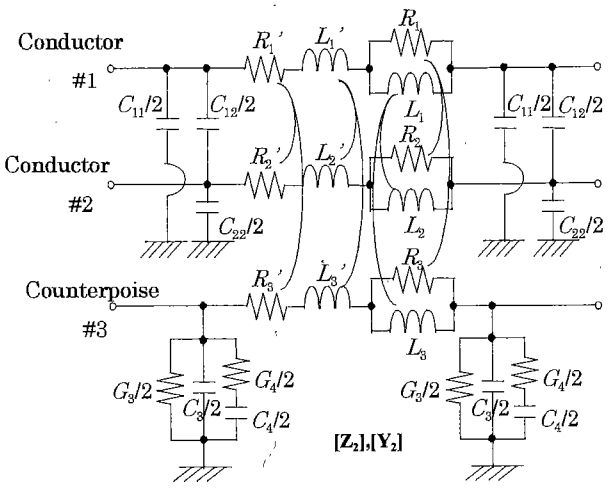

Fig. 11. A π equivalent circuit (Section ②)

counterpoise and overhead conductors.

Z_1 is given in eqs. (4), (6), and (9). The conductance and capacitance in terms of the shunt admittance, Y_1 of the counterpoise was given by Sunde [1] as follows:

$$\left.\begin{aligned} Y_1 &= G + j\omega C \\ G &= \frac{1}{\left(\frac{\rho_e}{\pi l}\right)\{\ln(2l/\sqrt{2rd}) - 1\}} \\ C &= \frac{\pi\varepsilon_0\varepsilon_r l}{\{\ln(2l/\sqrt{2rd}) - 1\}} \end{aligned}\right\} \cdots\cdots\cdots (10)$$

where, d: Buried depth of conductor, l: Length of conductor, r: Radius of conductor, ε_r: Permittivity of the ground

Note that eq. (10) is an approximation, as $l \gg d \gg r$, conductance G is the inverse of the steady state grounding resistance in a power frequency. A theoretical equation for high frequency is required to study this. Here, we used the next value.

$$G_3 = G_4 = G,\ C_3 = 5C_4 = C \cdots\cdots\cdots\cdots (11)$$

In $[Z_2]$ and $[Y_2]$ in section ②, the overhead conductors and counterpoise are represented for a three-phase distributed-parameter line. In such a case, the series impedance matrix and shunt admittance matrix are given by: -

$$\left.\begin{aligned} [Z_2] &= \begin{bmatrix} Z_{11} & Z_{12} & Z_{13} \\ Z_{21} & Z_{22} & Z_{23} \\ Z_{31} & Z_{32} & Z_{33} \end{bmatrix} \\ [Y_2] &= \begin{bmatrix} Y_{11} & Y_{12} & Y_{13} \\ Y_{21} & Y_{22} & Y_{23} \\ Y_{31} & Y_{32} & Y_{33} \end{bmatrix} \end{aligned}\right\} \cdots\cdots\cdots\cdots (12)$$

In the above equation, a 2×2 matrix is a two-phase overhead conductor. It is derived from eqs. (3) to (5) and (8) as $i, j = 1, 2$, or EMTP Cable Constants / Parameters. Z_{33} and Y_{33} are the same as Z_1 and Y_1 in sections ① and ③, respectively. Y_{13} and Y_{23} represent the mutual-admittance between the overhead conductor and counterpoise. Their value is zero as given by eq. (9). Z_{13} and Z_{23} represent the mutual-impedance

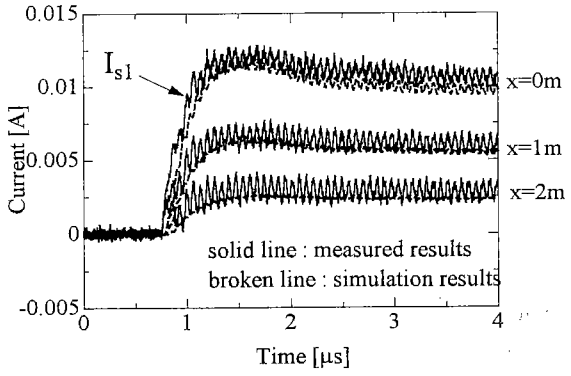

(a) Both ends open

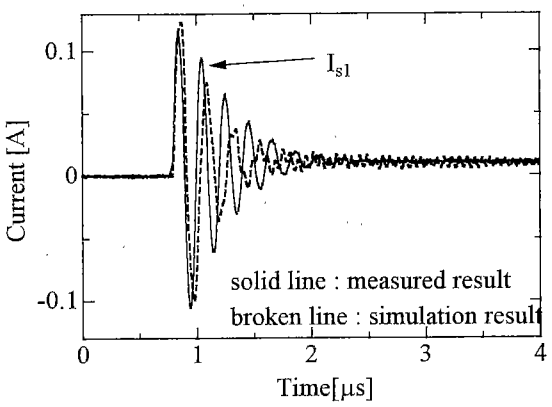

(b) Sending end grounded

Fig. 12. Comparison of measured and simulation results for induced current in a loop circuit

between the overhead conductor and the counterpoise. This depends on the switch condition, as given by eq. (7). Based on the method explained above, an EMTP simulation was carried out for the circuit illustrated in Fig. 9. The calculated result is shown in Fig. 12. This can be compared to the measured result, shown in Fig. 10.

The reasons for the difference between the simulation and measured results are explained as follows. As shown in Fig. 12(a), the voltage is induced in a loop circuit when the switches are opened at the both ends. The current flows due to the internal impedance of the conductor and was reflected between the sending and receiving ends of the loop circuit. This reflection is observed in the simulation and measured results, but the amplitude of the oscillation in the simulation is smaller than that in the actual measurement. This is due to the approximation of the conductor's internal impedance in eq. (4).

When the switch at the sending end is closed, the current from the counterpoise to the overhead conductor is also reflected between the receiving ends of the loop circuit and that of the counterpoise, via the sending end of the loop circuit. This oscillation is observed in Fig. 12(b). It is estimated that the difference in the oscillating period between the simulation and the measured result is due to a difference in the propagation velocity in the conductor, because the approximate equations of the impedance and the admittance are used. Also, the ground resistivity can be an important cause for the

difference, and the accuracy of the measured result is also one of reasons for the difference.

The proposed distributed line model is said to be satisfactorily accurate in comparison with the measurement results.

5. Conclusions

The following conclusions have been drawn, based on a field-test and a simulation — inducing characteristics from a counterpoise to a low-voltage control cable and an overhead loop circuit.

(1) A CVV-S cable is effective in reducing a voltage difference between cable core and grounding mesh, but that may not be reduced when a steep-front current is injected, when the cable sheath is not grounded at the other side of injected point.

(2) A CVV cable also has the effect of reducing a voltage difference between cable core and grounding mesh when a spare core is grounded at both ends.

(3) The proposed distributed line model of a counterpoise and overhead conductors is confirmed to be satisfactorily accurate in comparison with the measured results for a simulation of inducing characteristics.

(Manuscript received March 3, 2003,
revised June 26, 2003)

References

(1) E.D. Sunde: Earth conduction effects in transmission systems, Dover Pub., New York (1949)
(2) P.L. Bellaschi: "Impulse 60-cycle characteristics of driven grounds", *AIEE Trans.*, Vol.60, pp.123–128 (1941)
(3) P.L. Bellaschi, R.E. Armington, and A.E. Snowdon: "Impulse 60-cycle characteristics of driven grounds, PartII", *AIEE Trans.*, Vol.61, pp.349–363 (1942)
(4) K. Berger: "The behavior of earth connections under high intensity impulse currents", CIGRE 215 (1946)
(5) A.C. Liew and M. Darveniza: "Dynamic model of impulse characteristics of concentrated earth", *Proc. IEE*, Vol.121, pp.123–135 (1974)
(6) R. Kosztaluk, M. Loboda, and D. Mukhedkar: "Experimental study of transient ground impedance", *IEEE Trans. Power Apparatus Sgst.*, Vol.PAS-100, No.11, pp.4653–4660 (1981)
(7) E.E. Oettle: "A new estimation curve for predicting the impulse impedance of concentrated electrodes", *IEEE Trans. Power Apparatus Sgst.*, Vol.PWRD-3, No.4, pp.2020–2029 (1988)
(8) A.P. Meliopulos: Power system grounding and transients, Mercel Dekker Inc. (1988)
(9) S. Sekioka, T. Sonoda, Y. Kato, N. Nagaoka, and A. Ametani: "A time- and current-dependent grounding impedance model of a grounding net", *ICEE*, Vol.1, pp.832–835 (1998)
(10) T. Sonoda, H. Takesue, and S. Sekioka: "Measurements on surge Characteristics of Grounding Resistance of Counterpoises for Impluse Current", ICLP5.1 (2000)
(11) A. Ametani, N. Nayel, T. Sonoda, and S. Sekioka: "Basic Investigation of Wave Propagation Characteristics of an Underground Naked Conductor." *ICEE* (2002)
(12) S. Yamaguchi, A. Ametani, S. Sekioka, T. Sonoda, and Y. Kato: "A frequency-dependent counterpoise model for a transient analysis", Proc. ICEE'98, Vol.1, pp.753–756 (1998)
(13) S. Sekioka, T. Sonoda, Y. Kato, N. Nagaoka, and A. Ametani: "A time-and current-dependent grounding impedance model of a grounding net", Proc. ICEE'98, Vol.1, pp.832–835 (1998)
(14) A. Ametani: Distributed-Parameter Circuit Theory, Corona Pub. Co. (1990) (in Japanese)
(15) "Dielectric test voltages for low-voltage control circuits in power stations and substations", JEC-210 (1981) (in Japanese)
(16) Electrical Collaboration: Insulation design for low-voltage control circuit (1976) (in Japanese)
(17) S.A. Schelkunoff: "The electromagnetic theory of coaxial transmission line and cylindrical shields", *Bel System Tech. J.*, Vol.13, pp.532–579 (1934)
(18) F. Pollaczek: "Uber das Feld einer unendlich langen wechsel stromdurchflossenen Einfach leitung", *E.N.T.*, Band3, Heft9, pp.339–360 (1926)
(19) J.R. Carson: "The complex ground return plane : A simplified model for homogeneous and multi-layer earth return", *IEEE Trans. Power Apparatus Syst.*, Vol.PAS-100, No.8, pp.3686–3693 (1981)
(20) A. Deri, et al.: "The Complex ground return plane : A simplified model for homogeneous and multi-rayer earth return", *IEEE Trans. Power Apparatus Syst.*, Vol. PAS-100, No.8, pp.3686–3693 (1981)
(21) A. Ametani, S. Yamaguchi, and N. Nagaoka: "Mutual impedance between overhead and underground cables", EEUG'98 Proceedings, Czech (1998-11)

Appendix

Induced Voltage in the Loop Circuit

To obtain the induced voltage in the loop circuit on the ground due to the current that flows in the counterpoise, the current that flows in the counterpoise and the leak current from the counterpoise to the ground must be considered accurately. Maxwell's formulas are given by:

$$\nabla \times \boldsymbol{H} = \sigma \boldsymbol{E} + \varepsilon \partial \boldsymbol{E}/\partial t,\ \nabla \times \boldsymbol{E} = -\mu \partial \boldsymbol{H}/\partial t \quad \cdots\cdots\cdots\cdots\cdots (A1)$$

From eq. (A1),

$$\nabla^2 \boldsymbol{E} - \nabla(\nabla \boldsymbol{E}) = (j\omega\mu/\rho - \omega^2 \varepsilon \mu)\boldsymbol{E} \cdots\cdots (A2)$$

When true electric charge cannot exist, $\nabla \boldsymbol{E} = 0$.

Then, if displacement current is neglected, the following equation,

$$\nabla^2 \boldsymbol{E} = (j\omega\mu/\rho)\boldsymbol{E} \cdots\cdots\cdots\cdots\cdots\cdots\cdots (A3)$$

The electric field on the ground $\boldsymbol{E}_1$ and that in the ground $\boldsymbol{E}_2$ is supposed.

$$\partial \boldsymbol{E}_1/\partial x^2 + \partial^2 \boldsymbol{E}_1/\partial y^2 = \boldsymbol{0}\ (y \geq 0) \cdots\cdots\cdots (A4)$$

$$\partial^2 \boldsymbol{E}_2/\partial x^2 + \partial^2 \boldsymbol{E}_2/\partial y^2 = {m_2}^2 \boldsymbol{E}_2 + \rho {m_2}^2 \boldsymbol{I}\delta(x)\delta(y + y_c)\ (y \leq 0) \quad \cdots\cdots\cdots\cdots\cdots (A5)$$

Where ${m_2}^2 = (j\omega\mu/\rho)$

x: Horizontal distance between grounding mesh and overhead conductor [m]

y_c: Buried depth of counterpoise [m]

The tangential component of the field strength and the normal component of the electric flux density are the same, and from the boundary condition,

$$\frac{1}{\mu_1}\frac{\partial E_1}{\partial y} = \frac{1}{\mu_2}\frac{\partial E_2}{\partial y},\ \frac{\partial E_1}{\partial x} = \frac{\partial E_2}{\partial x},\ \frac{\partial E_1}{\partial z} = \frac{\partial E_2}{\partial z}\ (y = 0) \cdots\cdots\cdots\cdots\cdots\cdots (A6)$$

Eq. (A6) could be given. Eq. (A4) is solved using eqs. (A5) and (A6). The electric field on the ground being $E_1(x, y)$

$$E_{1Z}(x,y) = -j\omega\frac{\mu I}{2\pi}\int_{-\infty}^{\infty}\frac{\exp(-\sqrt{a^2+m_2{}^2}\cdot y_c - |a|\cdot y)}{|a|+\sqrt{a^2+m_2{}^2}} \times \exp(jax)da \quad \cdots\cdots\cdots\cdots\cdots\cdots \text{(A7)}$$

A square 1 [m] on one side of the loop circuit is defined, magnetic flex that interlinks the loop circuit is the only x-direction component

$$\Phi_x = B_x \cdot S = \mu l \int_{h_2}^{h_1} H_{1x}(x,y)dy \quad \cdots\cdots\cdots \text{(A8)}$$

Where B: Magnetic flex density [Wb/m^2],
S: Square measure of loop circuit [m^2]
$h_1 = h + l/2$ [m], $h_2 = h - l/2$ [m]

Then, induced voltage in the loop circuit $U(x)$ is given in the following equation as the time change in the magnetic flex interlinks the loop circuit.

$$\begin{aligned} U(x) &= -j\omega\Phi_x \\ &= -j\omega\mu l \int \left(\frac{\partial E_{1Z}(x,y)}{\partial y}\right) dy \\ &= -j\omega\frac{\mu l I}{2\pi}\int_{-\infty}^{\infty}\frac{\exp\left(-\sqrt{a^2+m_2{}^2}\cdot y_c\right)}{|a|+\sqrt{a^2+m_2{}^2}} \\ &\quad \times \{\exp(-ah_1) - \exp(-ah_2)\}\exp(jax)da \\ &\qquad\qquad \cdots\cdots\cdots\cdots\cdots \text{(A9)} \end{aligned}$$

Toshio Sonoda (Member) was born on July 15, 1965. He joined Kansai Electric Power, Osaka, Japan in 1984, and has engaged in the research of the electric power systems. He was awarded a Paper Prize from IEE of Japan in 2002.

Yasuo Takeuchi (Member) was born on May 5, 1947. He joined Kansai Electric Power, Osaka, Japan in 1966 and was a special student at the department of electrical engineering, Osaka University from 1970 to 1973. He has engaged in the research of the electric power systems.

Shozo Sekioka (Member) was born on December 30, 1963. He received the B. Sc. and Dr. Eng. degrees in electrical engineering from Doshisha University, Kyoto, Japan in 1986 and 1997, respectively. He joined Kansai Tech Corporation in 1987, and has been engaged in the lightning surge analysis in electric power systems.

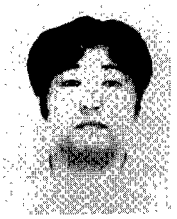

Noto Nagaoka (Member) was born on October 21, 1957. He received the B.Sc., M.Sc. and Dr. Eng. degrees from Doshisha University, Kyoto, Japan in 1980, 1982 and 1993, respectively. He was employed by Doshisha University in 1985 and presently he is a Professor at Doshisha University. He was awarded a Paper Prise from Ilum. Eng. Inst. in 1994. Dr. Nagaoka is a member of the IEEE and the IEE.

Akihiro Ametani (Member) was born on February 14, 1944. He received the B.Sc. and M.Sc. degrees from Doshisha University, Kyoto, Japan in 1966 and 1968, and the Ph.D. degree from University of Manchester, England in 1973. He was employed by Doshisha University from 1968 to 1971, the University of Manchester (UMIST) from 1971 to 1974, and also Bonneville Power Administration for summers from 1976 to 1981. He is currently a Professor at Doshisha University. He was awarded a Paper Prize from the IEE of Japan and Ilum. Eng. Inst. in 1977 and 1994 respectively. Dr. Ametani is a Fellow of the IEE and the IEEE, and Distinguished Member of CIGRE, and is a Chartered Engineer in the United Kingdom. He was the Chairman of the IEE Japan Centre, and is a Managing Director of the IEE of Japan.